— Original Paper —

3D dynamic crack propagation analysis with PDS-FEM

M.L.L. Wijerathne[1*], Hide Sakaguchi[1], Kenji Oguni[2], Muneo Hori[2]

This paper briefly explains a recently developed numerical technique called PDS-FEM and its dynamic extension. PDS-FEM is a simple and efficient numerical technique for modeling propagation crack in brittle materials. The discretization scheme used in this new numerical technique is called particle discretization scheme (PDS). PDS uses characteristic functions of Voronoi and Delaunay tessellations to discretize function and its derivatives, respectively. The uses of non-overlapping shape functions facilitate simple and numerically efficient failure treatment. We considered the dynamic extension of PDS-FEM and simulated several real life experiments, to illustrate the potential of simulating dynamic crack propagation of problems requiring fine domain discretizations.

Keywords : dynamic fracture, shock wave lithotripsy, PDS-FEM

Received 19 January 2009 ; Accepted 17 July 2009

1 Institute for Research on Earth Evolution, Japan Agency for Marine-Earth Science and Technology

2 Earthquake Research Institute, University. of Tokyo

Corresponding author :

M.L.L. Wijerathne

Institute for Research on Earth Evolution, Japan Agency for Marine-Earth Science and Technology

3173-25 Showa-machi, Kanazawa-ku, Yokohama 236-0001, Japan

+81-45-778-5972

lalith@jamstec.go.jp

1. Introduction

Some crack propagation problems require large scale simulations due to its nature; large domain of analysis, necessity of fine domain discretization due to the nature of the problem, necessity of Monte-Carlo simulations due to stochastic nature of the problem, etc.. A numerical method with efficient failure treatment is necessary for such large scale simulations. The existing continuum approaches, like cohesive traction methods, node splitting methods and element/nodal enrichment methods, involves numerically intensive failure treatments. A recently introduced numerical method called PDS-FEM (Hori *et al* (2005) and Wijerathne *et al* (2009)) provides simple and numerically efficient failure treatment, without adding new nodes or changing the mesh configuration. The failure treatment of PDS-FEM is light enough to apply to crack propagation problems requiring large scale simulations.

In this paper, we briefly explain the formulation of PDS-FEM and its dynamic extension. Simulation of dynamic crack propagation is of great practical importance in many fields of studies and challenging. To illustrate the potentials of the dynamic extension of PDS-FEM, we present a simulation of stone breaking in shock wave lithotripsy (SWL). In layman's term, SWL is how the doctors break kidney stones using external ultrasonic pulse. This method has been used nearly 30 years, but how the kidney stones break due to ultrasonic pulse induced water shock waves is still not well understood. We successfully simulated some of the crack patterns observed in SWL experiments. This problem is complicated since the initiation and propagation of the cracks are completely due to interfering stress waves in the solid and it involves very high strain rates (of the order 10^4 per second), shock waves, solid fluid interaction, etc.. According to the leading international researchers on SWL, this is the first time to reproduce such crack patterns. This pioneering result is a clear indication of the potentials of dynamic PDS-FEM in solving real life problems. In addition, we applied dynamic PDS-FEM to simulate failure of concrete wall under tsunami wave impact, etc..

We use the Cartesian coordinates and index notation, i.e., x_i stands for the i^{th} coordinate. The summation convention is employed, and $f_{,i}$ stands for the derivative $\partial f(\mathbf{x})/\partial x_i$.

2. PDS-FEM for modeling tensile failure in brittle solids

PDS-FEM is based on a non-conventional discretization scheme called particle discretization scheme (PDS), which uses a set of non-overlapping characteristic functions of two conjugate geometries Voronoi and Delaunay tessellations to discretize functions and its derivatives. Solving growing crack problems with PDS-FEM is straight forward and numerically efficient since the discontinuities in the discretized displacement field can be utilized to model displacement discontinuity across the crack surfaces, without introducing new nodes to accommodate the extending crack surface. One may doubt the accuracy of the solution of PDS-FEM since it uses discontinuous characteristic functions to model a smooth displacement field. It is straight forward to show that the stiffness matrix of PDS-FEM coincides with that of FEM with linear elements. Hence, the accuracy of nodal displacements of PDS-FEM is the same as that of FEM with linear element. In the rest of this document, only a brief description of PDS and PDS-FEM are given for the sake of completion and we refer to Hori *et al*. (2005) and Wijerathne *et al* (2009) for details.

Particle discretization scheme (PDS) uses a set of non-overlapping characteristic functions of two conjugate geometries (Fig. 1) to discretize functions and its derivatives. Using the set of characteristic functions $\phi^\alpha(\mathbf{x})$ of hypo-Voronoi diagrams $\{\Phi^\alpha(\mathbf{x})\}$, PDS discretize a function f defined over a domain as $f_d = \sum f^\alpha \phi^\alpha$, where the range of α is 1 to the number of hypo-Voronoi blocks. For a given set of mother points $\{x^\alpha\}$, hypo-Voronoi diagrams are

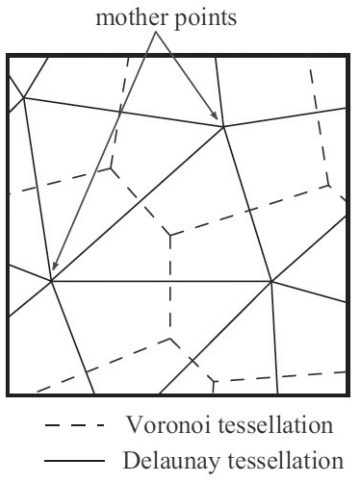

Figure 1: Conjugate geometries used in PDS

obtained by moving the common meeting point of neighboring three Voronoi diagrams to the center of gravity of the triangle formed by the three mother points of theVoronoi diagrams. Minimizing the discretization error $\int_B (f(x) - f^\alpha \phi^\alpha(x))^2 ds$, the coefficients f^α can be as $f^\alpha = \frac{1}{\Phi^\alpha} \int_{\Phi^\alpha} f(x) ds$. When it comes to the evaluation of derivatives of the discretized function f_d, the use characteristic functions results in unbounded derivatives eventually leading to problems of variational formulations. To circumvent these problems, an average value for $f_{,i} = \frac{\partial f_d^{\ \alpha}}{\partial x_i}$ is calculated using the Delaunay tessellation, Ψ^β , associated with Voronoi diagrams. Here, the range of index β is from 1 to the number of Delaunay triangles. When the derivatives, $f_{,i}$,, are discretized as $g_i = \sum g_i^\beta \Psi^\beta$, the coefficients g_i^β can be found as $g_i^\beta = \frac{1}{\Psi^\beta} \sum_\alpha \int_{\Psi^\beta} \phi_{,i}^\alpha \, ds$ by minimizing the error of discretization. This discretization of conjugate variables, functions and their derivatives, with the characteristic functions of conjugate geometries is called PDS.

2.1. PDS-FEM: spatial discretization

Implementation of PDS in FEM framework to solve the boundary value problem of solid is called PDS-FEM. We consider the implementation of PDS-FEM to solve the boundary value problem of linear elastic continuum, assuming infinitesimal deformations. As customary, the boundary value problem is posed as

$$\begin{cases} (c_{ijkl}(\mathbf{x})u_{k,l}(\mathbf{x}))_{,i} + b_j(\mathbf{x}) = \rho(\mathbf{x})\ddot{u}_j(\mathbf{x}) & \text{in } B \\ u_i(\mathbf{x}) = \bar{u}_i(\mathbf{x}) & \text{on } \partial B. \end{cases} \quad (1)$$

Here, c_{ijkl} is heterogeneous linear elasticity tensor, ρ is the density, b_i and $\bar{u}_i$ are the body forces and displacements prescribed in the body B and on the boundary ∂B, respectively. PDS-FEM uses the following functional of displacements, strain (ε_{ij}) and stress (σ_{ij}) to transform the above strong form the governing equations to an equivalent variational problem.

$$I(\mathbf{u}, \boldsymbol{\varepsilon}, \boldsymbol{\sigma}) = \int_B \frac{1}{2}\varepsilon_{ij} c_{ijkl} \varepsilon_{kl} - \sigma_{ij}(\varepsilon_{ij} - u_{j,i}) + b_i u_i - \frac{1}{2}\rho \dot{u}_i \dot{u}_i \, ds \quad (2)$$

It is straight forward to show that the first variations of I lead to the strong form given by Eq. 1.

Applying the PDS, the linear elastic domain B is discretized with Voronoi and Delaunay tessellation. Displacement field u_i and body forces b_i are discretized with $\{\phi^\alpha(\mathbf{x})\}$ as $u_i(\mathbf{x}) = \sum u_i^\alpha \phi^\alpha(\mathbf{x})$ and. $b_i(\mathbf{x}) = \sum b_i \phi^\alpha(\mathbf{x})$. The variables associated with derivatives σ_{ij}, ε_{ij} and c_{ijkl} are discretized in terms of $\{\psi^\beta\}$ as $\sigma_{ij}(x) = \sum \sigma_{ij}^\beta \psi^\beta(x)$, $\varepsilon_{ij}(x) = \sum \varepsilon_{ij}^\beta \psi^\beta(x)$ and $c_{ijkl}(x) = \sum c_{ijkl}^\beta \psi^\beta(x)$. Substituting these into I and setting $\partial I / \partial \varepsilon_{ij}^\beta = 0$ and $\partial I / \partial \sigma_{ij}^\beta = 0$, the discretization coefficients ε_{ij}^β and σ_{ij}^β are determined as $\sigma_{ij}^\beta = c_{ijkl}^\beta \varepsilon_{kl}^\beta$ and $\varepsilon_{ij}^\beta = \sum b_i^{\beta\alpha} u_j^\alpha$, where

$$b_i^{\beta\alpha} = \frac{1}{\Psi^\beta} \int_{\Psi^\beta} \phi_{,j}^\alpha(\mathbf{x}) ds. \quad (3)$$

Although $\phi_{,j}^\alpha$ is unbounded along $\partial\Phi^\alpha$, it is straight forward to evaluate $b_i^{\beta 1} = \frac{1}{2\Psi^\beta} \varepsilon_{ij3}(x_j^2 - x_j^3)$ with the aid of

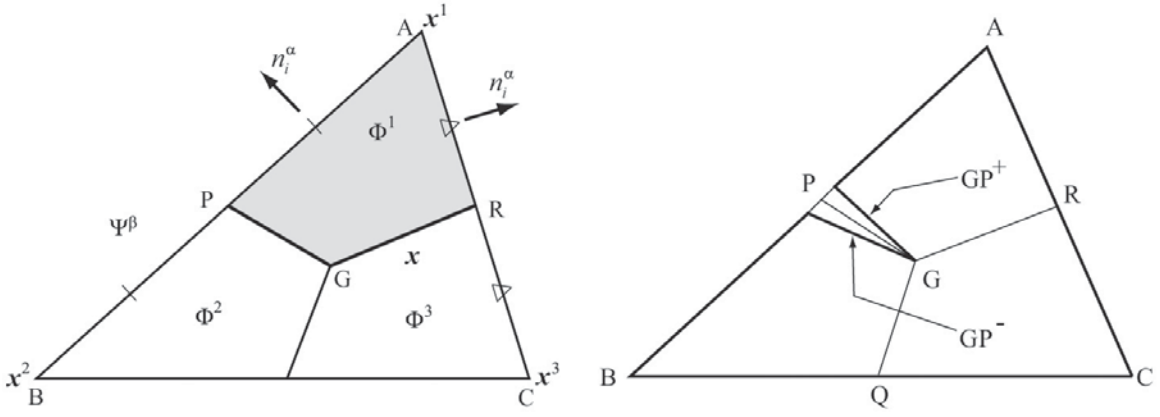

Figure 2: Evaluation of $b_j^{\beta\alpha}$ and approximate treatment of a crack growing along Voronoi block boundary PG

Gauss theorem (see Fig. 2a). Expressions for $b_i^{\beta 2}$ and $b_i^{\beta 3}$ can be obtained by suitably replacing thesuperscripts. Substituting these results to the discretized I and setting $\partial I/\partial u_i^\alpha = 0$, we obtain a linear set of equations for $\{u^\alpha\}$, as

$$\sum_{\alpha'} k_{ij}^{\alpha\alpha'} u_j^{\alpha'} - b_i^\alpha \Phi^\alpha = m^\alpha \ddot{u}_i^\alpha, \qquad (4)$$

where the element stiffness matrix

$$k_{ij}^{\alpha\alpha'} = \sum \Psi^\beta c_{ijkl}^\beta b_k^{\beta\alpha} b_l^{\beta\alpha'}. \qquad (5)$$

Eq. 4 is the governing matrix equation of FEM implemented with PDS, i.e., PDS-FEM. It is straight forward to show that the element stiffness matrix of PDS-FEM is exactly equal to that of FEM with linear triangular elements. Therefore, PDS-FEM has the same accuracy of FEM at nodal points.

2.2. Approximate Failure Treatment of PDS-FEM

PDS-FEM seeks for a numerically efficient treatment of modeling cracks in real materials, in which cracks bends and kink instead of following smooth paths. It uses existing discontinuities in the discretized displacement field to model propagating cracks. Even though homogeneous material properties are assumed, forcing cracks to propagate along the hypo-Voronoi boundaries makes the numerical model to be heterogeneous with respect to material strength; hypo-Voronoi blocks have infinite strength while their boundaries have a finite strength. Therefore, this treatment implicitly corresponds to the presence of local heterogeneity, like in real materials.

The approximate treatment is formulated as changes in elastic tensor c_{ijkl}. When a Voronoi block boundary is broken under tension, it is modeled by setting $c_{ijkl} = 0$ in an infinitesimally thin neighborhood, GP^+P^-, of the broken Voronoi block boundary , while c_{ijkl} is unchanged in the rest of the domain (see Fig. 2b). This changes the element stiffness matrix Eq. (5) of the broken element. This change of $k_{ij}^{\alpha\alpha'}$ is due to the fact that $b_i^{\beta\alpha}$, given by Eq. (3), drops the contribution from the derivative of the Voronoi characteristic function that appears in GP^+P^-.

Here, we briefly summarize the changes in $b_i^{\beta\alpha}$ due to the crack growing in a Delaunay triangle (see Fig. 2b). When GP is regarded as the new crack surfaces, the change in $b_i^{\beta\alpha}$ are $\Delta b_i^{\beta 1} = \frac{\varepsilon_{ij3}}{6}(2x_j^2 - x_j^3 - x_j^1)$, $\Delta b_i^{\beta 2} = -\Delta b_i^{\beta 1}$ and $\Delta b_i^{\beta 3} = 0$. All it needs to model a crack along GP is recomputing the element stiffness matrix with these changes to $b_i^{\beta\alpha}$ and updating the global stiffness matrix. For the cases when GQ or GR are the new crack surfaces, the changes of $b_i^{\beta\alpha}$ can be obtained by suitably replacing the superscripts.

The computational overhead associated with this approximate failure treatment is as small as recomputing an element stiffness matrix and applying the changes to the global matrix. Obviously, this approximate treatment of PDS-FEM is numerically efficient compared to common FEM approaches like accommodating a new crack surface by introducing new nodes or enriching the test functions with Heaviside function.

For the sake of simplicity, only the 2D case has been explained in this short paper. Extension of PDS-FEM to 3D is straight forward with hypo-Voronoi diagram and the associated Delaunay tessellation in 3D and extending the range of subscripts from (1, 2) to (1, 2, 3), in Eq. 4 and 5.

2.3. Time integration

For the time integration of Eq. (4), any standard time integration method like Newmark-beta, Verlet methods, AVI, etc. can be applied. In addition, there is a rich set of symplectic, energy momentum preserving algorithms used in particle physics. These are higher order accurate, suitable for long time integrations, and can deal with steep potentials which would be useful in dealing with sudden changes in the system like dynamic crack propagation.

Due to the non-overlapping shape functions used in discretization process, the domain discretized with PDS can be can be interpreted as modeling a continuum with a collection of particles. The interactions of these particles are defined by the stiffness matrix. We exploited this particle representation of the discretized model of PDS-FEM and implemented a time integration algorithm from particle physics called Candy's method (Candy et al (2009)). It's forth order accurate symplectic and energy momentum preserving.

Denoting the mass and velocity of hypo-Voronoi block Φ^α with m^α and $\dot{u}_i^\alpha$, the kinetic energy and the potential energy can be written as $T(\dot{u}) = \frac{1}{2}\sum m^\alpha \dot{u}_i^\alpha \dot{u}_i^\alpha$ and $V(u) = \frac{1}{2}\sum_{\alpha'} k_{ij}^{\alpha\alpha'} u_i^\alpha u_j^{\alpha'}$. Hamiltonian for this collection of particles can be written as $H = p_i \dot{u}_i - L$, where $L = T - V$ is the Lagrangian and the generalized momentum are $\dot{p}_i^\alpha = \partial L/\partial \dot{u}_i = m^\alpha \dot{u}_i^\alpha$. Now the Hamiltonian for our set of

particles can be written as

$$H = \frac{1}{2}\sum_{\alpha} m^{\alpha}\dot{u}_i^{\alpha}\dot{u}_i^{\alpha} + k_{ij}^{\alpha\alpha'}u_i^{\alpha}u_j^{\alpha'} \qquad (6)$$

For our separable Hamiltonian, Candy's method is given by

$$\mathbf{p}^k = \mathbf{p}^{k-1} + b^k F(\mathbf{q}^{k-1})\Delta t$$
$$\mathbf{q}^k = \mathbf{p}^{k-1} + a^k P(\mathbf{p}^{k-1})\Delta t \qquad k = 1,...,4,$$

where $F(\mathbf{q}) = -\partial V(\mathbf{q})/\partial \mathbf{q}$, $P(\mathbf{p}) = \partial T(\mathbf{p})/\partial \mathbf{p}$, Δt *is* the time increment and *k* is an iteration counter. The constants a_k and b_k for Candy's method are $a_1=a_4=(2+2^{1/3}+2^{-1/3})/6$, $a_2=a_3=(1-2^{1/3}-2^{-1/3})/6$, $b_1 = 0$, $b_2 = b_4 = 1/(2-2^{1/3})$ and $b_3 = 1/(2-2^{2/3})$. When started with known conditions $p^1 = p(t_{n-1})$, $q^1 = q(t_{n-1})$ at time t_{n-1} , state at time t_n is given by p^4 and q^4, after four iterations.

2.3.1. Failure criterion for Dynamic extension

The dynamic fracture phenomenon is not instantaneous and it requires certain time. When subjected to dynamic loading, the crack propagation strongly depends on both the stress wave amplitude and the exposure time. For simulating dynamic brittle fracture, we adopted the Tuler-Butcher (Nyoungue et al., 1995) failure criterion, which can be expressed as

$$\int_0^{t_f} (\sigma_1 - \sigma_0)^{\beta} dt \geq K_f .$$

Here, $\sigma_1 \geq \sigma_0 \geq 0$ where σ_1 is the maximum principal stress, σ_0 is a specific threshold stress, t_f is time for the fracture and K_f is the stress impulse for failure. In the absence of correct values of β, t_f, σ_0 and K_f for the material of interest, we assumed $\beta = 2$ and σ_0=14 MPa while some values for K_f ad t_f are assumed such that they generate experimentally observed crack patterns.

3. Shock wave lithotripsy as an example of 3D dynamic PDS-FEM

In this section, we present the successful regeneration of crack patterns observed in a shock wave lithotripsy (SWL) related experiment, as an illustrative example of dynamic PDS-FEM. Shock wave lithotripsy is the fragmentation of kidney stones by focusing an ultrasonic pressure pulse onto the stones. By repetitively applying an ultrasonic pulse, the stone is broken into small enough pieces so that they can be passed naturally. First introduced in early 80's, SWL is the main treatment for kidney stones, presently (Robin et al., 2005; Zhou et al., 2002). Irrespective its long history, the mechanism of stone fragmentation has not been well understood and fundamentally the modern SWL instruments are not much different from the early 80's design (Xi et al., 2001; Robin et al., 2005; Oleg et al., 2007; Zhou et al., 2002). Ray tracing and high speed photoelasticity have been used to locate the possible high stress regions (Xi et al., 2001). However, these methods cannot be used to study the crack evolution under dynamic stress fields in kidney stones. Numerical studies of SWL stone fragmentation are significantly important on its future developments. To authors' knowledge no successful simulation of SWL stone fragmentation has been reported, to date.

We successfully applied the dynamic extension of

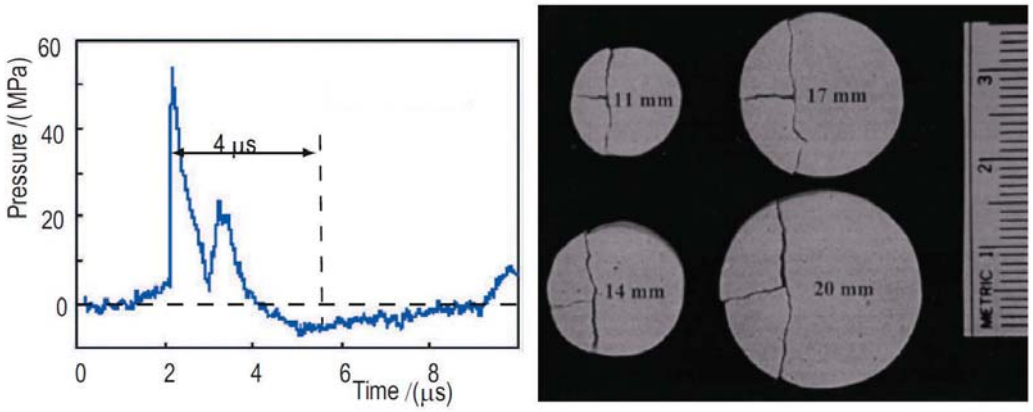

(a) (b)

Figure 3: A typical pressure pulse induced in water due to the ultrasonic pulse in SWL (source Zhou et al., 2002) and T-shaped cracked plaster of Paris samples (source Xi et al., 2001)

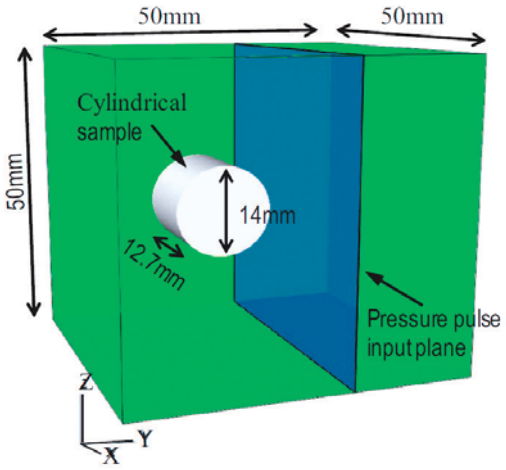

Figure 4: ConFiguration of the numerical model

Table 1: Material properties used in SWL simulation

	Plaster of Paris	Water
Young's modulus /(GPa)	8.875	
Poisson's ratio	0.228	
Bulk modulus /(GPa)		2.2
P wave velocity /(m⁄s)	2478	1483
S wave velocity /(m⁄s)	1471	0

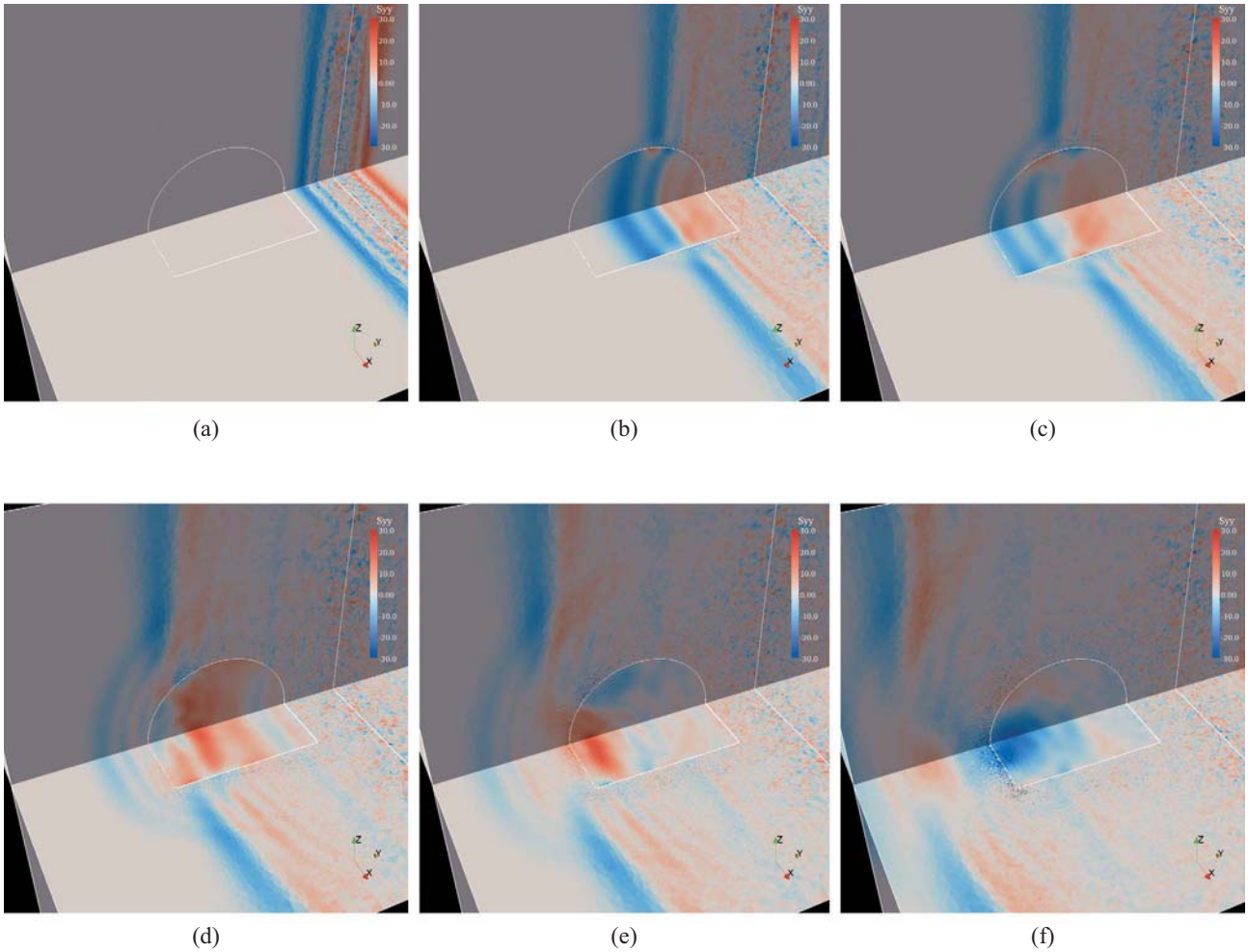

(a) (b) (c)

(d) (e) (f)

Figure 5: Time evolution of pressure in water and σ_{yy} in the solid sample. Red stands for tension and blue for compression

PDS-FEM to simulate an interesting set of fragmentation experiments reported in Xi et al. (2001). Here, we briefly explain the experiments reported in Xi et al. (2001) and suggest referring the original paper for details. In their experiments, different shaped samples made of plaster of Paris are immersed in a water tank and an ultrasonic pressure pulse is focused onto the sample. A typical pressure pulse induced in water due to the ultrasonic pulse is shown in Fig. 3a. The induced pressure pulse in water consists of initial short and high intense compressive phase and a long and low intense tensile phase.

One of the interesting results reported in Xi et al. (2001) is the T-shaped fragmentation of a cylindrical sample as shown in Fig. 3b. Figure 4 shows the geometric details of the numerical model used for simulating this cylinder fragmentation. A rectangular domain of 50 × 50 × 50mm is considered to be filled with water and a cylindrical sample of radius 7mm and length 12.7mm is immersed. The water domain surrounding the cylindrical sample is modeled by setting $\mu = 0$, where λ and μ are the Lame's constants. The material properties of water and plaster of Paris are given in table 1. The spatial variation of the water pressure pulse has been observed not to change appreciably in the vicinity of the sample. Therefore, a plane pressure wave pulse is used as the input to the simulation by applying the pressure pulse profile shown in Fig. 3a on the blue color plane shown in Fig. 4. In order to correctly capture the stress waves generated by short compression phase of nearly 1μs period, the model is discretized to nearly 6 million tetrahedral elements.

Figure 5 shows some snap shots of water pressure and σ_{yy} components in the solid. Figure 5a shows the compressive phase of the incoming pressure pulse. Once the pressure pulse hit the solid, the induced P-wave font starts to moves ahead of water pressure pulse (see Fig. 5b), since the V_p of plaster of Paris is larger than that of water. This creates shock waves in water (which are not clear in these small Figures). As observed in the high speed photoealstic experiments, the P-wave front become broader compared to that of water. The induced shear waves in solid moves almost at the same sped of water pressure waves. When the solid P-wave reflects from the distal surface, it undergoes a phase change and becomes tensile. Also, it starts to focus due to the circular shape of the reflecting surface, leading to increase in amplitude of the focusing tensile pressure pulse. This focusing and interference with the 4μs lagging tensile phase generates, large tensile region as shown in Fig. 5d and 5e. This high stress region sparks the initial crack.

When exposed to multiple pressure pulses, cylindrical samples of various sizes have been observed to break into three parts with T-shaped crack profiles. The experimentally observed T-shaped crack profiles are shown in Fig. 3b. Just as observed in the experiment, when exposed to multiple pressure pulses, the cylindrical sample of the numerical simulation broke into three parts with T-shaped crack profiles (see Figure 6). Figure 6 shows the crack profile of the numerical simulation at several sections. In Figure 6, the number at the bottom right of each sub-Figure indicates the distance from the center of the cylinder (+ and - stands for the left and right). As can be clearly seen, PDS-FEM successfully reproduces the crack patterns observed in SWL experiments. Also, the distance to the vertical crack from the distal surface is nearly equal to that observed in the experiment. Similarly, we reproduced the crack patterns for rectangular prism reported in (Xi et al., 2001).

Compared with most of the dynamic crack propagation phenomena triggered by static loading this SWL

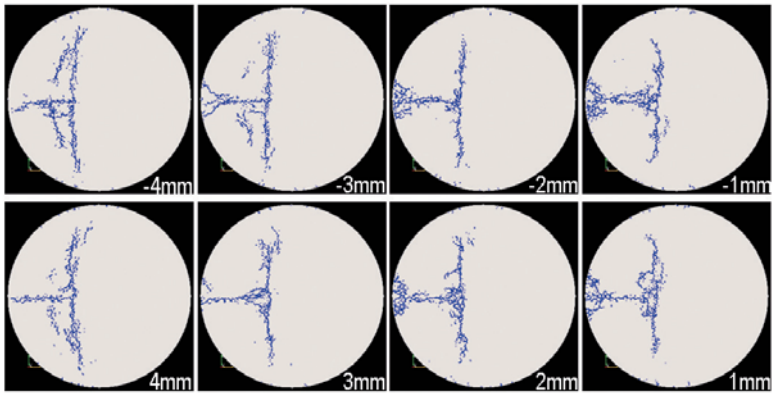

Figure 6: Numerically simulated crack patterns. The number stands for the distance from the center.

experiment is complicated. Unlike in many other examples, the solid body does not undergo any global large enough deformation to generate sufficient stress level for failure and there are no macroscopic initial cracks. The fragmentation is completely due to interference of high intense stress waves which are responsible for both the initiation and propagation of cracks. The successful reproduction of the crack patterns of these SWL experiments is a clear indication of the potential of PDS-FEM to simulate complicated 3D dynamic problems.

4. Concluding remarks

This paper presents a brief introduction to PDS-FEM and its dynamic extension. Because of its simple and numerically efficient failure treatments, PDS-FEM is a great tool for crack propagation simulations of large scale problems. With a parallel code, we simulated several experimentally observed crack patterns observed. The successful reproduction of crack patterns of SWL experiment, briefly explained in this paper, is a clear indication of the potentials of PDS-FEM. We are expecting further develop and apply PDS-FEM to understand various fracture involved phenomena like concrete wall failure under tsunami wave impact, shear crack propagation on pre-known surfaces, etc..

References

Candy, J., W. Rozmus(1991), A Symplectic Integration Algorithm for Separable Hamiltonian Functions, *J. Comput. Phys., 92*, 230.

Cleveland, R. O. and O. A. Sapozhnikov (2005), Modeling elastic wave propagation in kidney stones with application to shock wave lithotripsy, *J. Acoust. Soc. Am., 118 (4)*, 2668-2676.

Hori, M., K. Oguni, H. Sakaguchi(2005), Proposal of FEM implemented with particle discretization for analysis of failure phenomena, *J. of Mech. and Phy. of Solids, 53(3)*, 681-703.

Liu Y. and P. Zhong (2002), BegoStone-new stone phantom for shock wave lithotripsy research, *J. Acoust. Soc. Am*., 112 (4), 1265-1268.

Nyoungue, A., Z. Azari, M. Abbadi, S. Dominiak and S. Hanim (2005), Glass damage by impact spallation, *Materials Science and Engn. A*, 407(1-2), 256-264.

Sapozhnikov, O. A., A. D. Maxwell, B. MacConaghy, and M. R. Bailey(2007), A mechanistic analysis of stone fracture in lithotripsy, *J. Acoust. Soc. Am*., 121 (2),1190- 1202.

Wjerathne, M. L. L., K. Oguni and M. Hori (2009), Numerical analysis of growing crack problems using particle discretization scheme, *Int. J. for Numerical Methods in Eng*. DOI 10.1002/nme.2620.

Xi, XF and P. Zhong (2001), Dynamic photoelastic study of the transient stress field in solids during shock wave lithotripsy, *J. Acoust. Soc. Am., 109 (3)*, 1226-1239.

Zhou, YF and P. Zhong (2002), The effect of reflector geometry on the acoustic field and bubble dynamics produced by an electrohydraulic shock wave lithotripter, *J. Acoust. Soc. Am*., 119 (6), 3625-3636.